Force approximation for a plasma actuator operating in atmospheric air

Kunwar Pal Singh and Subrata Roy[a)]
Computational Plasma Dynamics Laboratory and Test Facility, Department of Mechanical and Aerospace Engineering, University of Florida, Gainesville, Florida 32611, USA

(Received 27 August 2007; accepted 6 November 2006; published online 10 January 2008)

A plasma actuator has been studied using a self-consistent multibody system of quiescent air, plasma, and dielectric. Equations governing the motion of charged and neutral species have been solved with Poisson's equation. Based on first principles analysis, a functional relationship between electrodynamic force and electrical and physical control parameters has been approximated and numerically tested for air. The magnitude of approximated force increases with the fourth power of the amplitude of rf potential. Thus, the induced fluid velocity also increases. The induced velocity shows momentum injection very close to the actuator surface. There is, however, a very small increase in the induced velocity with the forcing frequency. For the specific range of operational parameters considered, the proposed force relation may help speed up the plasma actuator design process. © *2008 American Institute of Physics*. [DOI: 10.1063/1.2827484]

I. INTRODUCTION

Plasma actuators have demonstrated the ability to promote boundary layer attachment on airfoils at a high angle of attack. Experiments and simulations have shown that the momentum boundary layer is significantly influenced in low speed regime due to plasma actuation. The dielectric barrier discharge (DBD) plasma actuator is a simple device, as shown in Fig. 1, with two electrodes separated by a dielectric and staggered in the flow direction. These electrodes are subjected to an alternating bias of several thousand volts at a frequency in the range of kilohertz. Such device holds the promise of increasing lift and/or reducing drag of airfoils and fuselages through electronic means.

In a DBD plasma actuator, Townsend avalanche may dominate characteristics of plasma producing microdischarges which dominate the force production. The V-dot probe technique shows that the voltage across the plasma is less than half of that is applied across the electrodes.[1] The dynamics of fluid flow and heat transfer can be actively induced by such discharge at atmospheric pressure. Force production of a plasma actuator was experimentally measured in a large vacuum chamber,[2] and a linear relationship between force production and air pressure was found. Pavon *et al.*[3] investigated different bulk airflow velocities, plasma excitation frequencies, and voltages and found that the bulk airflow has a significant influence on the plasma characteristics. The temporal force and the time-averaged body force have been measured for a range of frequencies and voltages. The results show that for a constant voltage, the spatially averaged body force is proportional to frequency and the impulse per cycle is constant. At constant frequency, the increase in body force with voltage was shown.[4] The pressure was found to be higher in the downstream of the electrode due to the ion and large fluid particle interaction. A clear dependence of the induced jet velocity on the applied voltage and frequency was found.[5] The actuator power can be reduced by 90% and its durability can be improved by operating it in an unsteady manner.[6]

Measurements by Enloe *et al.* indicate that the momentum coupling between the charged particles and the neutral particles occurs on time scales much shorter than that for the bulk fluid motion.[7] They suggest treating the actuator as a heat and momentum input device into a small control volume. There are different kinds of power losses such as reactive power losses due to inadequate impedance matching of the power supply to the actuator, dielectric heating, and power required to maintain the atmospheric pressure plasma during the operation of plasma actuator. These power losses need to be minimized.[8] Recently, Kuryachii has shown that the maximum gas velocity induced by discharge tends to limiting values. Transverse component of the body force may play an important role in an increase in longitudinal gas velocity.[9]

The multiple-scale processes such as convection, diffusion, and reaction/ionization mechanisms make the continuity equations of the plasma dynamics stiff. Jayaraman *et al.* have used a sequential finite-volume operator-split algorithm capable of conserving space charge to handle the stiffness.[10] The computed body force field based on DBD formulation of Roy and Gaitonde[11] gave improved description compared to

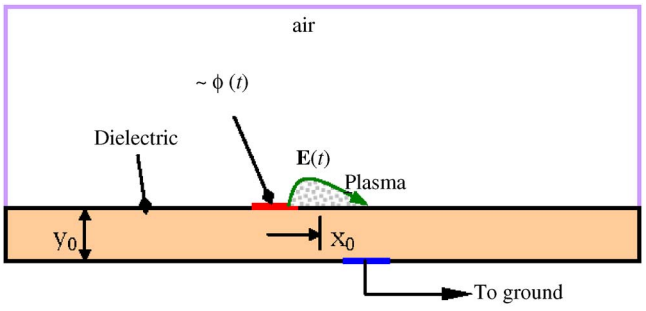

FIG. 1. (Color online) Schematic of the asymmetric single dielectric barrier plasma actuators operating in air.

[a)]Electronic mail: roy@ufl.edu.

an analytical-empirical treatment.[12] An attached wall jet-type flow capable of modifying the near wall flow structures attributed to the body force field on the fluid flow was found.

Such first principles modeling of plasma actuators operating in atmospheric air requires solving continuity equations of different species, Poisson's equation, and Navier-Stokes equations self-consistently.[11,13] This requires very long computational time and is rather expensive. If we can *adequately* approximate the electrodynamic force for direct implementation into Navier-Stokes equations, the significant cost of solving plasma equation can be saved. The challenge, however, is to find an adequate description of the force that actuates the neighboring flow.

In the present work, we employ first principles simulations to approximate spatial dependence of the electrodynamic force imparted to air as a function of the amplitude of rf potential and the interelectrode spacing. The predictions using this approximated force are then validated for nine cases using the first principles equations governing the dynamics of charged and neutral species of air. We have given the geometry description in Sec. II. Numerical details in Sec. III describe initial and boundary conditions. Section IV discusses simulation results. Conclusions are drawn in Sec. V.

II. GEOMETRY DESCRIPTION

Figure 1 shows the schematic of the simulation region which is 3 cm long and 5 mm high. The region includes an asymmetric single dielectric barrier plasma actuator consisting of two electrodes separated by a dielectric. The upper electrode is exposed to the air, while the lower electrode is placed underneath the dielectric. The lower part of the domain consists of a 1 mm thick insulator with relative dielectric constant $\varepsilon_r=10$, while the upper part is filled with air of relative dielectric constant $\varepsilon_r=1.0055$. We have assumed negligible thickness for the electrodes. The powered electrode extends from $x=1.2$ to 1.4 cm at $y=1$ mm, and the grounded electrode is from 1.6 to 1.8 cm at $y=0$. There is a 2 mm gap between rf and grounded electrodes along the x axis. An alternating potential of $\phi=\phi_0 \sin(2\pi ft)$ in volts is applied to the exposed electrode. We have chosen a small domain to save computational time. The domain is big enough for plasma equations from Debye length consideration; however, it may be limiting for fluid boundary layer using Navier-Stokes equations.

We have studied nine cases in this article with $\phi_0=800$, 1000, and 1200 V, and $f=2.5$, 5, and 10 kHz. For the air chemistry, we have neglected metastable species along with N^{4+} and O^{4+} due to their extremely high recombination rates. Also, the numerical complexity is further simplified by excluding nitrous oxide. The model equations governing chemistry of discharge, the drift-diffusion form of continuity, and Poisson equations for the electrons, ions, and neutrals have been reported earlier.[13]

The electron temperature is calculated from $\mathbf{E}=k_B T_e/(\nabla n_e/n_e)$, which is obtained assuming an initial Boltzmann distribution, $n_e \propto \exp(e\phi/k_B T_e)$. The secondary electron emission from the exposed surface is taken as a function of incident electron energy[14] and remains small, i.e., less than 10^{-3}. No material sputtering of the surface is considered. The bulk density of air is taken to be 1.2 kg/m^3.

III. NUMERICAL DETAILS

The all initial particle concentrations, except those of the electrons and nitrogen and oxygen molecules, are assumed to be 0. Atmospheric ratio of 3.6 is taken for nitrogen to oxygen gas molecules. Initial oxygen molecule density is taken as $10^{26}/m^3$, and the electron density is taken as $10^9/m^3$. Initial rf potential is 0. We have chosen zero initial neutral velocities (quiescent gas flow). These initial conditions have been chosen to match with the realistic experimental conditions. The solution is sensitive to the initial conditions; however, we report the results for the chosen initial conditions.

The boundary conditions for Poisson's equation are as follows: The potential is applied to the exposed electrode with $\phi=\phi_0 \sin(2\pi ft)$ in volts. The embedded electrode is grounded. The electric insulation condition (normal component of electric field equal to zero) is assumed at the outer boundaries of the domain. The electric field normal to the dielectric surface is discontinuous by the separated charge. The boundary conditions related to continuity equations of air species are as follows: The currents flow normal only to the rf electrode since it is an equipotential surface. Homogeneous Neumann conditions are applied to the outer edges of the domain and electric insulation is assumed at the surface of the dielectric. The currents flow normal as well as parallel to the dielectric surface. No slip boundary conditions have been applied at dielectric surface for Navier-Stokes equations. Neutral boundary conditions have been applied at outer boundaries.

The two-dimensional air dielectric barrier discharge in an asymmetric geometry has been solved using a Galerkin variational formulation based finite element method[15] to efficiently model the multiscale problem. We have solved governing equations for densities and velocities of electron, ion, and neutral species of nitrogen and oxygen, and the electric potential. The time step size is taken adaptive with the longest step of hundred times of dielectric relaxation time scale to capture fast response time of the electrons. An element size smaller than Debye length has been chosen close to the rf electrode to properly resolve spatial dependences of the variables.

We have shown earlier[13,15] that the electrodynamic force ($q\mathbf{E}$) is the highest close to the overlap or displacement region between exposed rf electrode and grounded electrode. With that knowledge and assuming that an essentially time-averaged body force interacts with air, the electrodynamic force has been approximated by following equation:

$$\mathbf{F} = F_{x0}\phi_0^4 \exp(-\{[x-x_0-(y-y_0)]/y\}^2 - \beta_x(y-y_0)^2)\hat{i} + F_{y0}\phi_0^4 \exp\{-[(x-x_0)/y]^2 - \beta_y(y-y_0)^2\}\hat{j}. \quad (1)$$

The values of F_{x0} and F_{y0} are taken from the average electrodynamic force obtained by solving air-plasma equations. The functional relationship with the fourth power of potential is based on plasma simulation that will be elaborated later. As shown in Fig. 1, x_0 is the midpoint between the rf

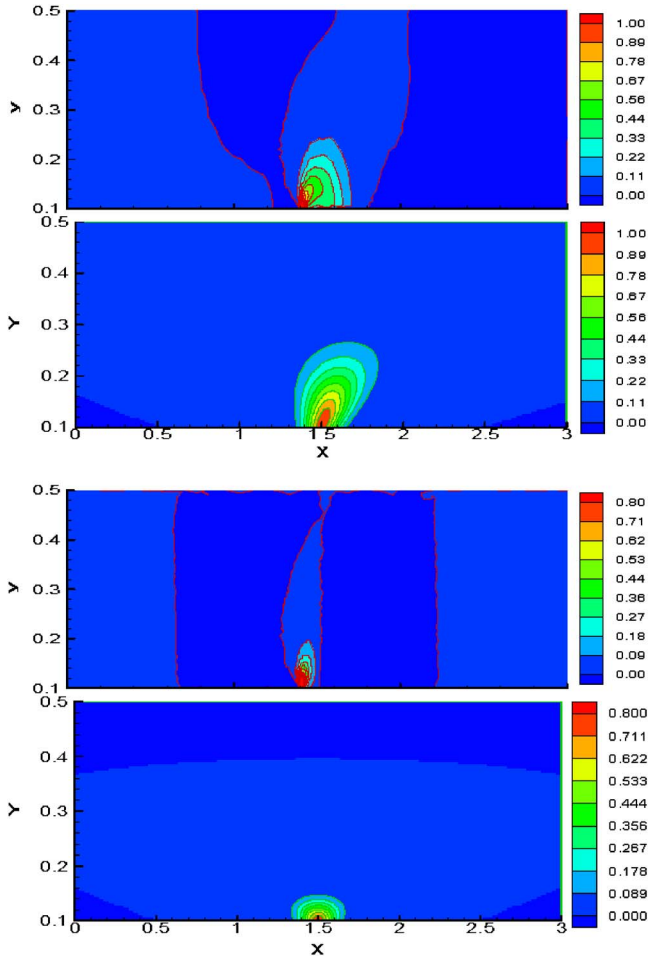

FIG. 2. (Color online) (a) The x component and (b) the y component of the normalized electrodynamic force and the normalized approximated force for $f=5$ kHz and 1000 V.

electrode and the grounded electrode, and y_0 is at the dielectric surface. The values of β_x and β_y are functions of dielectric material and adjusted to match the velocity induced by electrodynamic force.

IV. RESULTS AND DISCUSSION

Nine cases have been studied in this article with the amplitudes of applied rf potential $\phi_0=800$, 1000, and 1200 V and the frequencies of rf potential $f=2.5$, 5, and 10 kHz. For these cases, in Eq. (1), we use $F_{x0}=2.6$, $F_{y0}=2.0$, $x_0=0.015$ m, $y_0=0.001$ m, $\beta_x=8\times10^5$, and $\beta_y=10^7$. The upper part of each figure in Figs. 2–7 is obtained using electrodynamic force from numerical solution of air-plasma equations and the lower part is obtained using an approximated force in Navier-Stokes equations. The force and velocity components have been normalized by the maximum values of these quantities.

Figures 2(a) and 2(b) compare the profiles of x and y components of the normalized electrodynamic force computed from plasma equations and the approximated force given by Eq. (1) for $f=5$ kHz and 1000 V. It can be seen that there is an agreement between the force distributions. Figures 3(a)–3(d) show x and y components of the normalized electrodynamic force and approximated force as a function of x at different locations of y for $f=5$ kHz and 1000 V. The

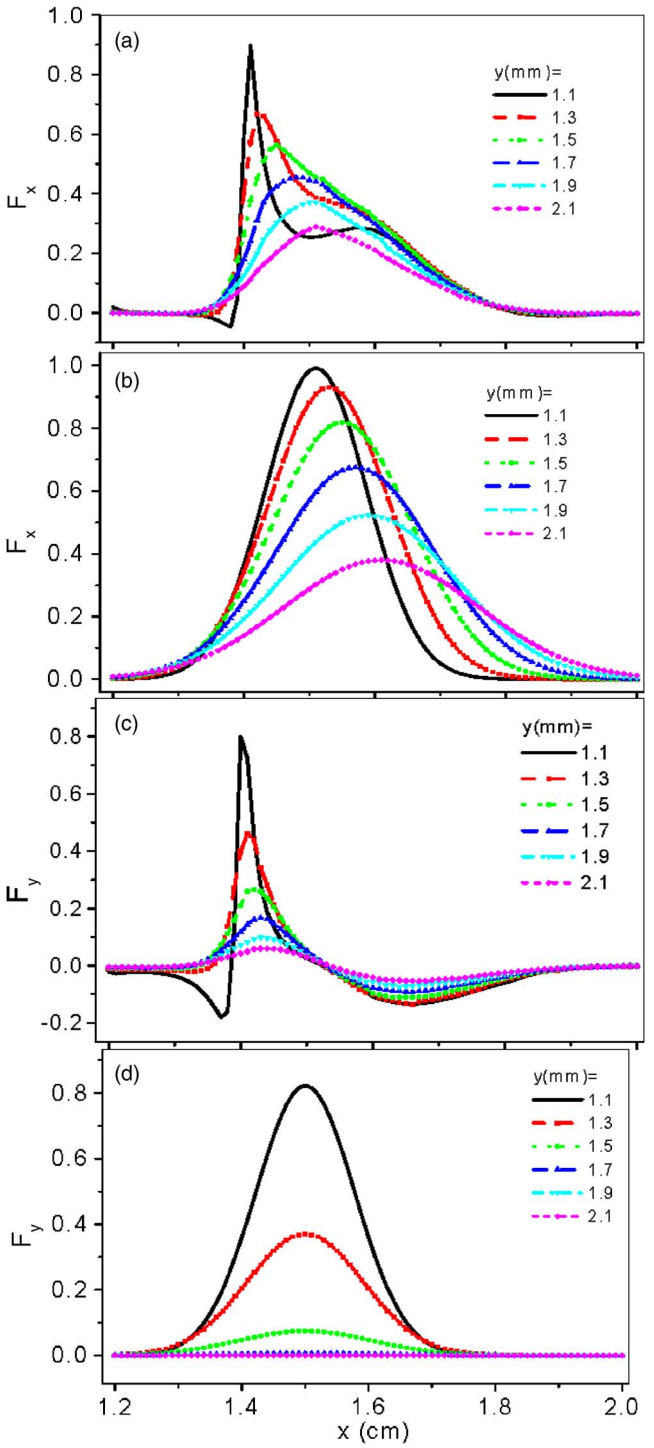

FIG. 3. (Color online) The x component of the normalized (a) electrodynamic force and (b) approximated force. The y component of the normalized (c) electrodynamic force and (d) approximated force as a function of x at different locations of y for $f=5$ kHz and 1000 V.

combined effect of higher electric field, higher ionization, and higher charge separation results in fourth of dependence of the electrodynamic force on the potential. Even though the approximated force is not exactly equal to the electrodynamic force, its effect on induced velocity is nearly the same. This can be seen from the following results.

Figures 4(a)–4(c) show profiles of the x component of the normalized velocity for 800, 1000, and 1200 V, respectively, at $f=5$ kHz. The x component of normalized velocity

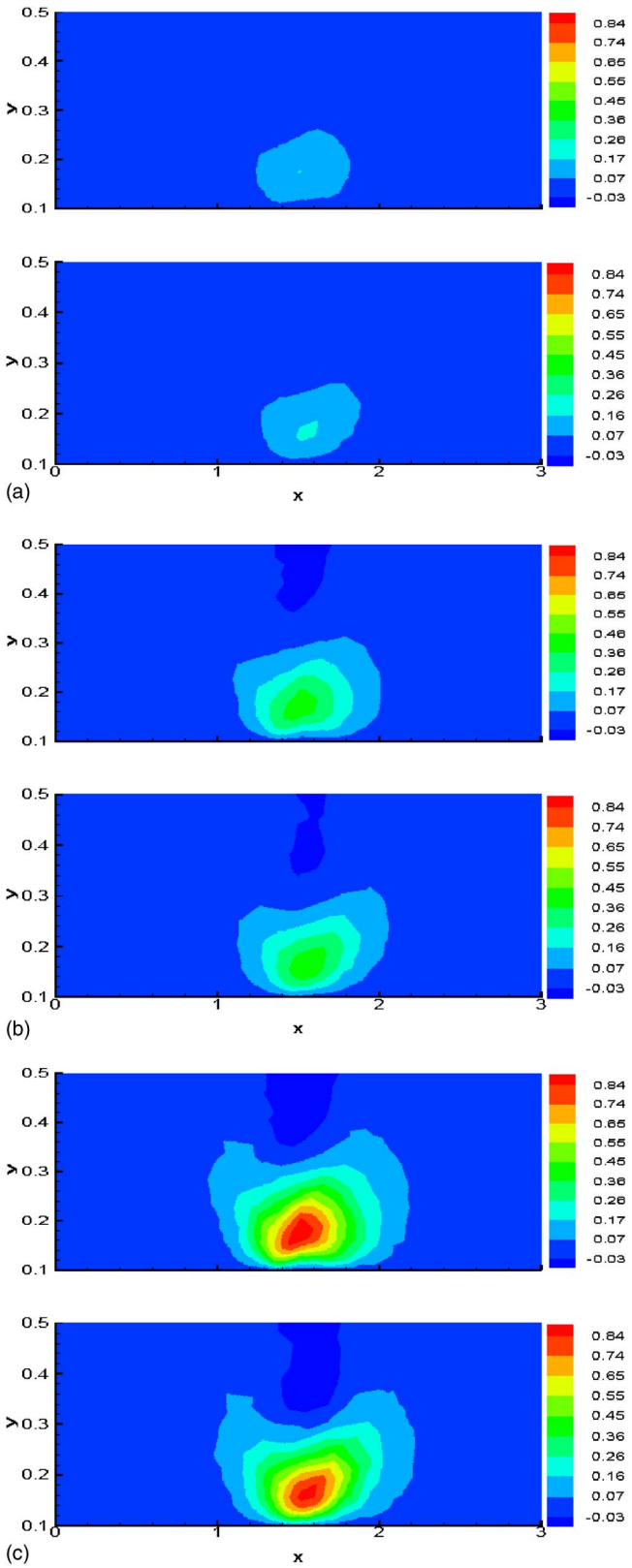

FIG. 4. (Color online) The x component of the normalized velocity obtained using electrodynamic force and approximated force for $f=5$ kHz for (a) 800, (b) 1000, and (c) 1200 V.

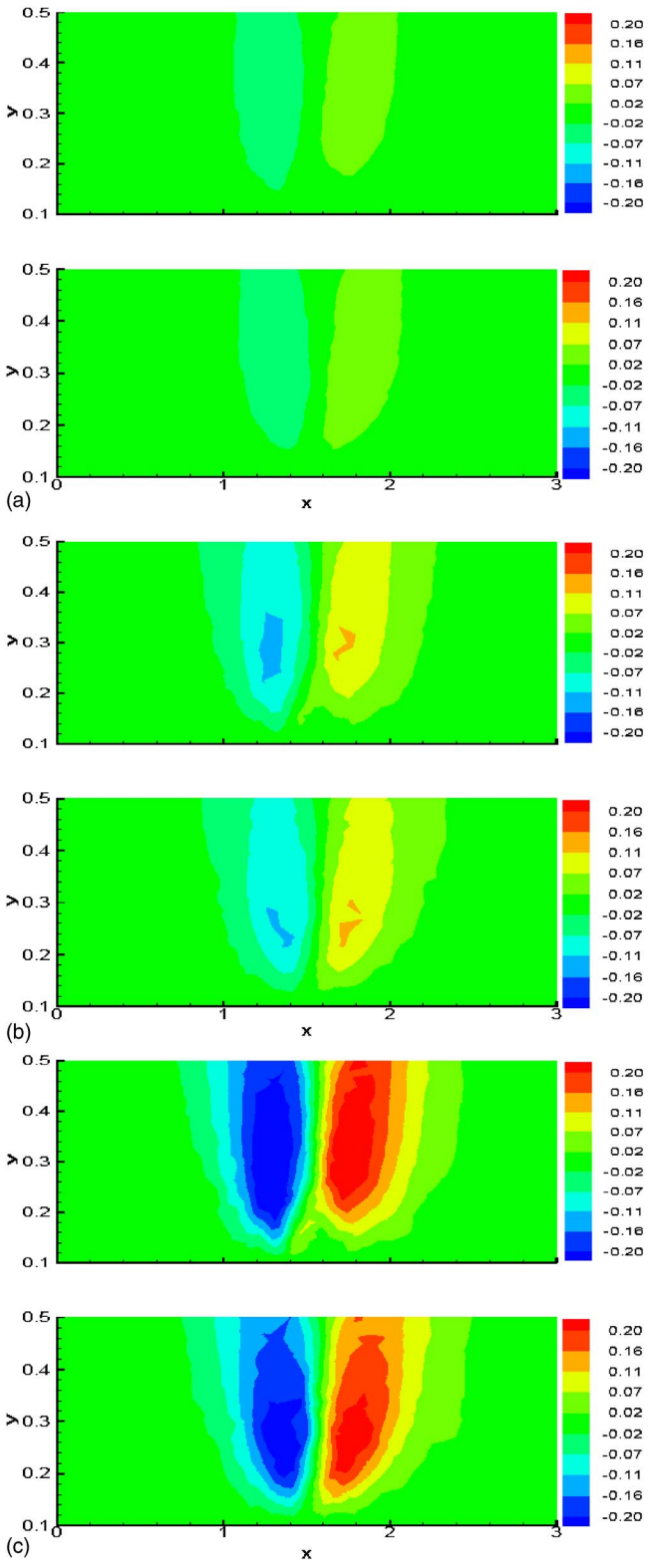

FIG. 5. (Color online) The y component of the normalized velocity obtained using electrodynamic force and approximated force for $f=5$ kHz for (a) 800, (b) 1000, and (c) 1200 V.

profiles shows a reasonable agreement between the solutions obtained using electrodynamic force from air-plasma equations and the solutions obtained using an approximated force. Figures 5(a)–5(c) show profiles of y component of the normalized velocity at $f=5$ kHz for 800, 1000, and 1200 V, respectively. Again, the y component of the normalized velocity profiles also shows a reasonable agreement between the solutions obtained using electrodynamic force from air-plasma equations and the solutions obtained using an approximated equation for the force. Figures 6(a)–6(c) show

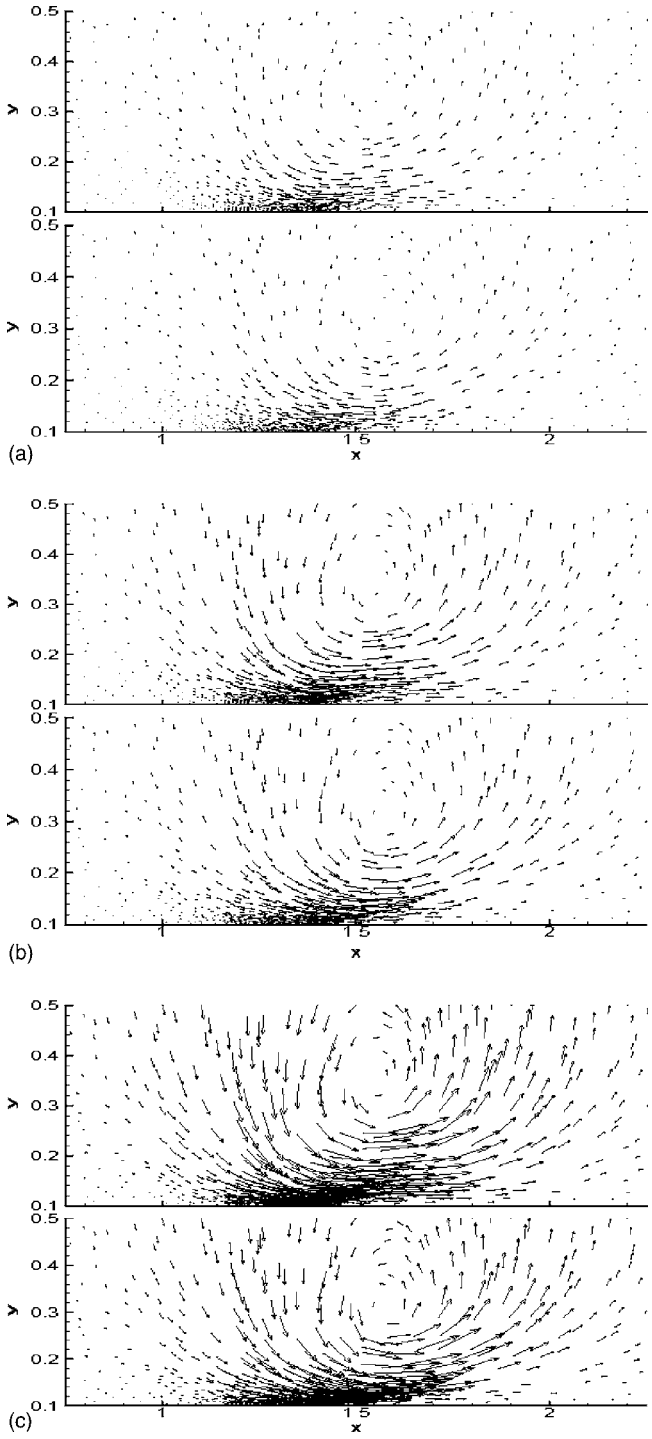

FIG. 6. The velocity vectors obtained using electrodynamic force and approximated force for $f=5$ kHz for (a) 800, (b) 1000, and (c) 1200 V.

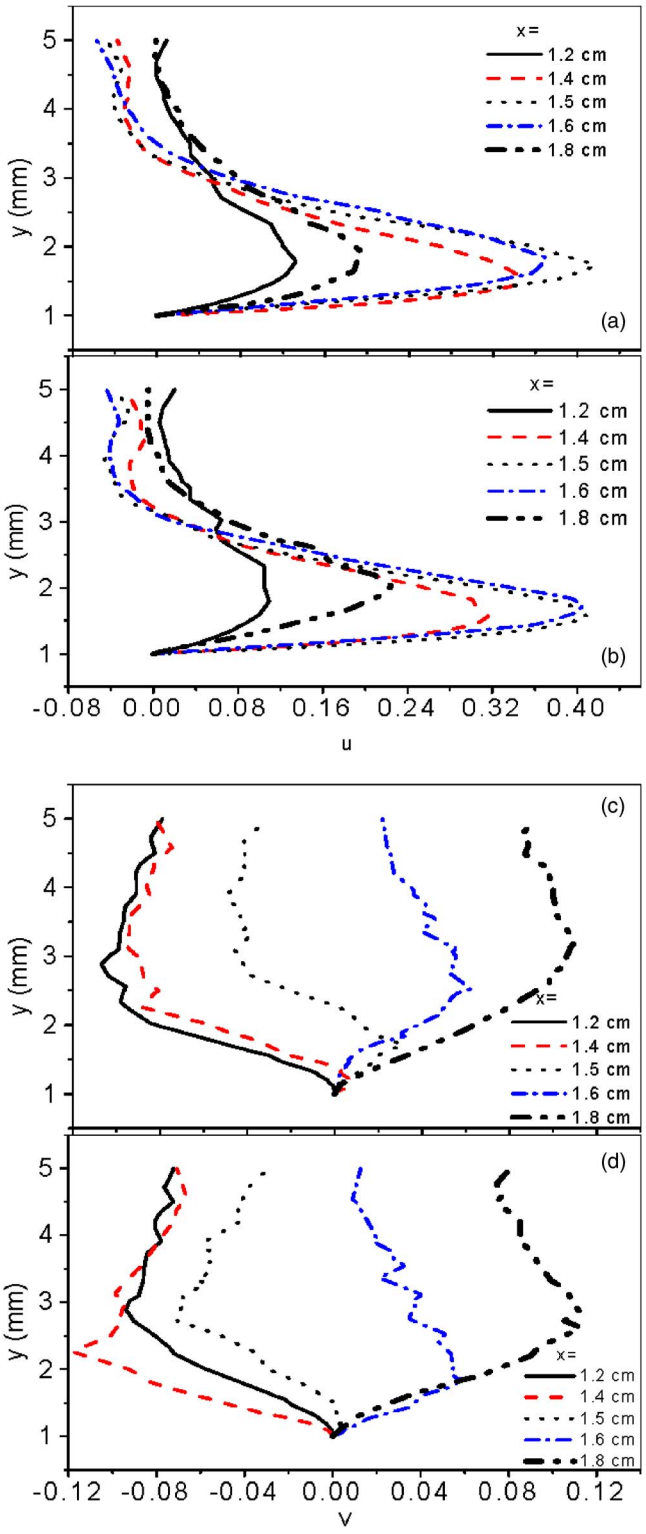

FIG. 7. (Color online) The normalized velocity components obtained using electrodynamic force and approximated force as a function of y for different locations of x for $f=5$ kHz and 1000 V.

velocity vectors at $f=5$ kHz for 800, 1000, and 1200 V, respectively. It can be seen that there is a reasonable agreement between the velocity vectors obtained using electrodynamic force from air-plasma equations and the approximated force. Figure 7 shows the normalized velocity components obtained using electrodynamic force and the approximated force as a function of y for different locations of x for $f=5$ kHz and 1000 V. It can be seen that there is good agreement between the normalized velocity distributions. These results again confirm that the approximated force is reasonably correct as it induces approximately the same normalized velocity. The approximated force is not exactly equal to the actual electrodynamic force; hence, there is qualitative difference between the near wall velocity profiles. The approximated force can be used in Navier-Stokes equations and the effect of the plasma actuator can be predicted. This provides a faster way

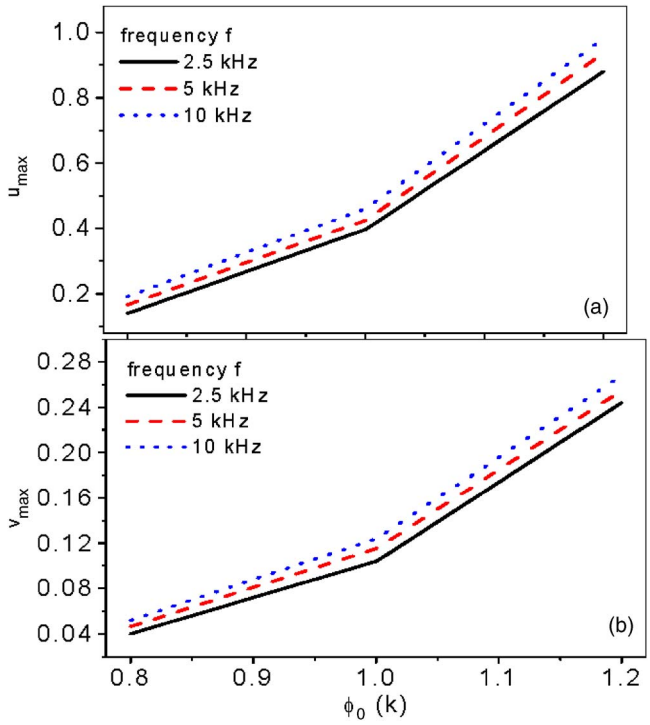

FIG. 8. (Color online) The maximum normalized velocity as a function of the amplitude of the applied rf voltage ϕ_0 in kilovolts for $f=2.5$, 5, and 10 kHz, (a) the x component of the normalized velocity u_{max} and (b) the y component of the normalized velocity v_{max}.

of modeling the discharge effect without solving air-plasma equations and Navier-Stokes equations self-consistently.

Figures 8(a) and 8(b) show the x and y components of the maximum normalized velocities u_{max} and v_{max} as a function of the amplitude of the applied rf potential ϕ_0 for three frequencies $f=2.5$, 5, and 10 kHz. The electrodynamic force obtained from the solution of air-plasma equations has been used in Navier-Stokes equations to obtain these velocities. It can be seen that the induced normalized velocity increases with the applied rf potential. A higher rf potential generates a higher electric field which causes a higher ionization and a higher charge separation. An increase in average electrodynamic force results in a higher induced velocity. The velocity increases with the frequency of applied rf potential as well; however, the increase is very small. The dependence of induced velocity on frequency of the applied rf potential is in agreement with the results of Roth and Dai.[8] The electric field, level of ionization, and charge separation do not change much with the frequency of the applied rf potential; hence, the average electrodynamic force and the induced velocity also respond weakly.

V. CONCLUSIONS

We have approximated the spatial dependence of the electrodynamic force based on the first principles calculations for air. The *approximate force* is a fourth order polynomial of applied rf potential and is a function of the actuator geometry. The coefficients are calibrated with the study of a plasma actuator under nine conditions using a self-consistent multibody system of quiescent air, plasma, and dielectric. The approximated force equation induces very similar spatial profiles of velocity as compared to that computed from plasma equations. The magnitude of induced velocity increases with the amplitude of operating rf potential. The induced velocities are not affected much by the frequency of applied rf potential. This should be explored further. The induced velocity shows mostly acceleration above the actuator. While the presented force approximation is valid only for the operational parameters reported in this article, such force relation may become helpful in efficiently simulating exploratory designs of plasma actuators. For general parameters and different actuator configurations, first principles simulation remains necessary.

[1] G. I. Font, C. L. Enloe, T. E. McLaughlin, and D. Orlov, Proceedings of the 45th AIAA Aerospace Sciences Meeting and Exhibit, Reno, Nevada, 2007 (AIAA, Washington, D.C., 2002), Paper No. AIAA 2007-188.
[2] J. W. Gregory, C. L. Enloe, G. I. Font, and T. E. McLaughlin, Proceedings of the 45th AIAA Aerospace Sciences Meeting and Exhibit, Reno, Nevada, 2007 (AIAA, Washington, D.C., 2002), Paper No. AIAA 2007-185.
[3] S. Pavon, J.-L. Dorier, Ch. Hollenstein, P. Ott, and P. Leyland, J. Phys. D **40**, 1733 (2007).
[4] C. O. Porter, J. W. Baughn, T. E. McLaughlin, C. L. Enloe, and G. I. Font, Proceedings of the 44th AIAA Aerospace Sciences Meeting and Exhibit, Reno, Nevada, 9–12 January 2006 (AIAA, Washington, D.C., 2002), Paper No. AIAA 2006-104.
[5] A. Santhanakrishnan and J. D. Jacob, J. Phys. D **40**, 637 (2007).
[6] T. C. Corke, B. Mertz, and M. P. Patel, Proceedings of the 44th AIAA Aerospace Sciences Meeting and Exhibit, Reno, Nevada, 9–12 January 2006 (AIAA, Washington, D.C., 2002), Paper No. AIAA 2006-1208.
[7] C. L. Enloe, T. E. McLaughlin, G. I. Font, and J. W. Baughn, Proceedings of the 44th AIAA Aerospace Sciences Meeting and Exhibit, Reno, Nevada, 9–12 January 2006 (AIAA, Washington, D.C., 2002), Paper No. AIAA 2006-166.
[8] J. R. Roth and X. Dai, Proceedings of the 44th AIAA Aerospace Sciences Meeting and Exhibit, Reno, Nevada, 9–12 January 2006 (AIAA, Washington, D.C., 2002), Paper No. AIAA 2006-1203.
[9] A. P. Kuryachii, Fluid Dyn. **41**, 366 (2006).
[10] B. Jayaraman, S. Thakur, and W. Shyy, J. Heat Transfer **129**, 517 (2007); Proceedings of the 44th AIAA Aerospace Sciences Meeting and Exhibit, Reno, Nevada, 9–12 January 2006 (AIAA, Washington, D.C., 2002), Paper No. AIAA 2006-686.
[11] S. Roy and D. V. Gaitonde, Proceedings of the 43rd AIAA Aeropsace Sciences Meeting, 10–13 January, 2005, Reno, NV (AIAA, Washington, D.C., 2002), Paper No. AIAA 2005-160.
[12] W. Shyy, B. Jayaraman, and A. Andersson, J. Appl. Phys. **92**, 6434 (2002).
[13] K. P. Singh and S. Roy, J. Appl. Phys. **101**, 123308 (2007).
[14] S. Roy and B. P. Pandey, Phys. Plasmas **9**, 4052 (2002).
[15] S. Roy and D. Gaitonde, Phys. Plasmas **13**, 023503 (2006); S. Roy, B. P. Pandey, J. Poggie, and D. Gaitonde, *ibid.* **10**, 2578 (2003).